Optimization of Xenon Biosensors for Detection of Protein Interactions

Thomas J. Lowery,[a, b] Sandra Garcia,[a, c] Lana Chavez,[a, c] E. Janette Ruiz,[a, c] Tom Wu,[d] Thierry Brotin,[e] Jean-Pierre Dutasta,[e] David S. King,[f] Peter G. Schultz,[d] Alex Pines,[a, c] and David E. Wemmer*[a, b]

Hyperpolarized ^{129}Xe NMR spectroscopy can detect the presence of specific low-concentration biomolecular analytes by means of a xenon biosensor that consists of a water-soluble, targeted cryptophane-A cage that encapsulates the xenon. In this work, we use the prototypical biotinylated xenon biosensor to determine the relationship between the molecular composition of the xenon biosensor and the characteristics of protein-bound resonances. The effects of diastereomer overlap, dipole–dipole coupling, chemical-shift anisotropy, xenon exchange, and biosensor conformational exchange on the protein-bound biosensor signal were assessed. It was found that an optimal protein-bound biosensor signal can be obtained by minimizing the number of biosensor diastereomers and using a flexible linker of appropriate length. Both the line width and sensitivity of chemical shift to protein binding of the xenon biosensor were found to be inversely proportional to linker length.

Introduction

Recent advances in nanomaterials and magnetic-resonance polarization techniques have led to the development of new types of magnetic-resonance imaging (MRI) contrast agents that provide for greater sensitivity and higher selectivity. Proton-relaxation agents have been biochemically targeted to yield imaging signals that report the presence of specific molecules. Examples include detecting and imaging biomolecular binding events and enzyme activity with functionalized magnetite nanoparticles[1] and imaging gene expression with chemically modified paramagnetic ions.[2] Polarization-enhanced contrast agents have also been used to obtain extraordinary definition of perfused blood and tissue volumes. Dynamic nuclear polarization-enhanced glucose has been used for angiography,[3] and polarized helium and xenon for lung and tissue imaging.[4] Polarized nuclei offer high sensitivity, low-background signal, and relatively long relaxation times.

Unlike proton-relaxation agents, which have been conjugated to target specific tissue types or biomolecules for achieving selective contrast, polarized nuclei have thus far only been used in a nonspecific manner in which signal localization relies on slow transport and tissue barriers. One means of targeting polarized nuclei to a specific analyte or sample region uses a molecular adaptor, termed a xenon biosensor. This sensor was developed as a means to "functionalize" polarized xenon in aqueous solutions and target it to report on a specific biomolecular target or event. The prototypical xenon biosensor consists of three parts, a xenon-binding cryptophane-A cage, a short peptide for water solubility, and a moiety that binds a specific biomolecule. A biotinylated sensor was used to demonstrate that the biosensor-bound xenon resonances significantly broaden and shift downfield in the presence of avidin.[5–6] The sensitivity of biosensor-encapsulated xenon to its local environment indicates that "functionalized" xenon can serve as a magnetic-resonance reporter for targeted in situ biosensing and imaging.[7]

Our initial biotinylated cryptophane-A construct (1, Scheme 1) gave rise to four narrow ^{129}Xe resonances when free in solution. These four resonances derive from the four diastereomers RLL, RLR, LLL, and LLR that arise from the chirality of the three biosensor components, the cage, peptide, and maleimide.[6] In the absence of protein, two of the diastereomer resonances almost completely overlap with the other two, yield-

[a] T. J. Lowery, S. Garcia, L. Chavez, E. J. Ruiz, Prof. A. Pines, Prof. D. E. Wemmer
Department of Chemistry, University of California at Berkeley
Berkeley, CA 94720 (USA)
Fax: (+1) 510-486-6059
E-mail: DEWemmer@lbl.gov

[b] T. J. Lowery, Prof. D. E. Wemmer
Physical Biosciences Division, Lawrence Berkeley National Laboratory
1 Cyclotron Road, Berkeley, CA 94720 (USA)

[c] S. Garcia, L. Chavez, E. J. Ruiz, Prof. A. Pines
Material Sciences Division, Lawrence Berkeley National Laboratory
1 Cyclotron Road, Berkeley, CA 94720 (USA)

[d] T. Wu, Prof. P. G. Schultz
Department of Chemistry and The Skaggs Institute for Chemical Biology
The Scripps Research Institute
10550 North Torrey Pines Road, La Jolla, California 92037 (USA)

[e] Dr. T. Brotin, Dr. J.-P. Dutasta
Laboratoire de Chimie de l'ENS-Lyon (UMR 5182 CNRS/ENS-Lyon)
46 Allée d'Italie, 69364 Lyon 07 (France)

[f] Dr. D. S. King
Department of Molecular and Cell Biology and
Howard Hughes Medical Institute, University of California at Berkeley
Berkeley, CA 94720 (USA)

Supporting information for this article is available on the WWW under http://www.chembiochem.org or from the author.
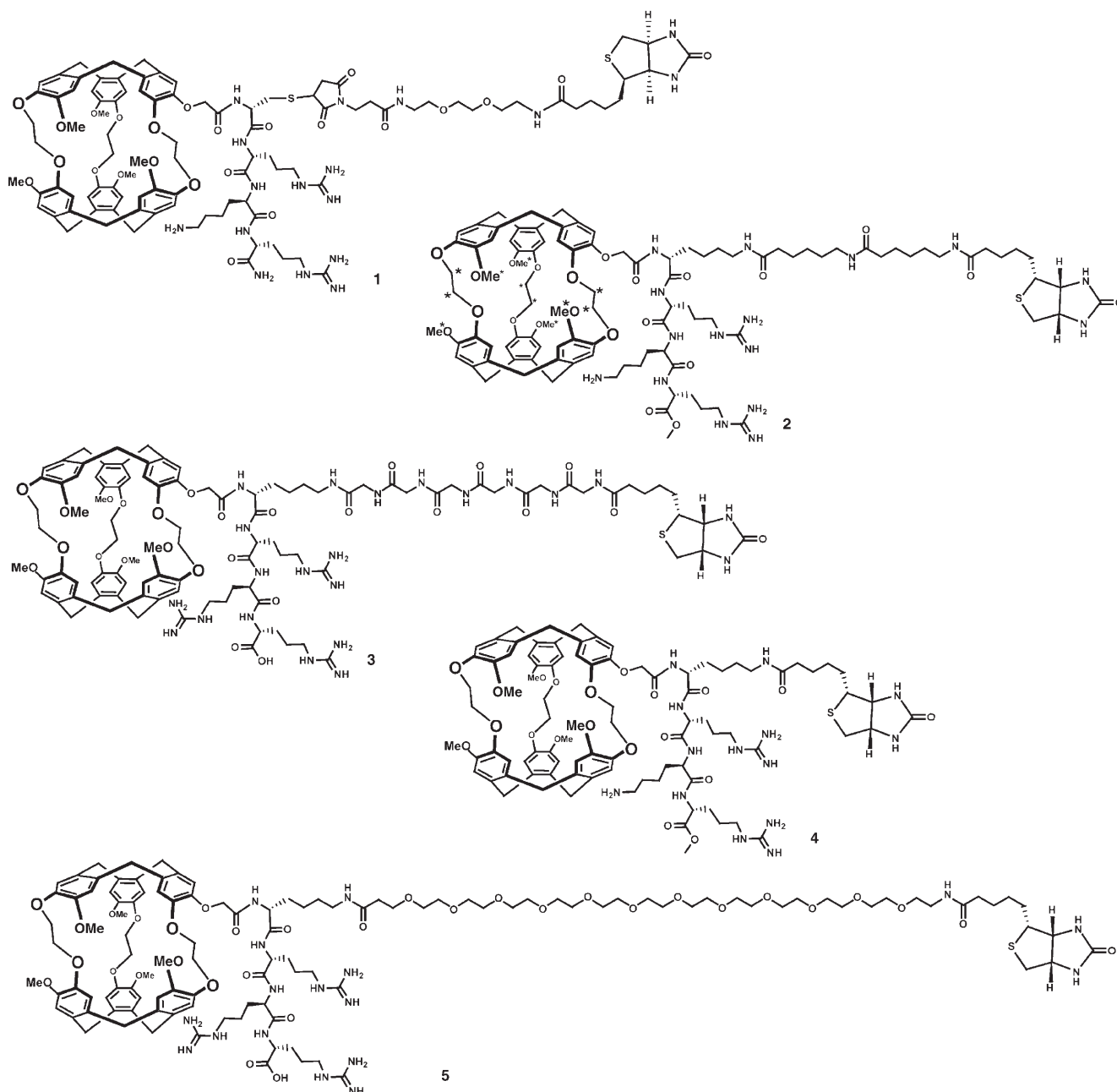
Scheme 1. The five biotinylated xenon biosensor constructs that were synthesized and characterized.

ing two slightly separated peaks of 20 Hz total line width.[6] The avidin-bound form of **1** yielded a single broad peak ~200 Hz in line width that was shifted ~2 ppm downfield (Figure S1 in the Supporting Information). The broadening observed upon binding appears to arise from an increase in correlation time through a combination of relaxation mechanisms.[6]

We envision applications of functionalized xenon to include spatially localized sensing of specific molecules (e.g. metabolites, antigens, etc.) in a selective and low-background manner by tethering a xenon-binding cage to a selective affinity tag,

such as an antibody, or a small-molecule sensor, such as a ligand-binding protein.[6,7] Such applications require acquiring signal from a biomolecule-bound xenon biosensor. The large line width observed for the protein-bound prototype sensor would significantly limit detection sensitivity. To address this issue, we have prepared and determined NMR characteristics of six different biotinylated xenon biosensors when bound to avidin. Through these studies we identify the molecular features that impart optimal line width and sensitivity to biosensor applications.

Results and Discussion

Diastereomers

The contribution of a change in the distribution of diastereomer resonances upon protein binding was investigated by reducing the number of biosensor diastereomers from four to two by replacing the cysteine maleimide linkage between the cage peptide and the biotinylated linker in **1** with a lysine–amide bond linkage. This new biosensor construct, **2**, has only two diastereomers, *RL* and *LL*. When this biosensor was titrated with avidin, the two diastereomeric peaks shift downfield from 65.1 and 64.5 ppm with line widths of 24 and 25 Hz, respectively, to 67.9 and 66.4 ppm with line widths of 43 and 35 Hz, respectively (Figure 1). Avidin binding to **2** shifts the downfield
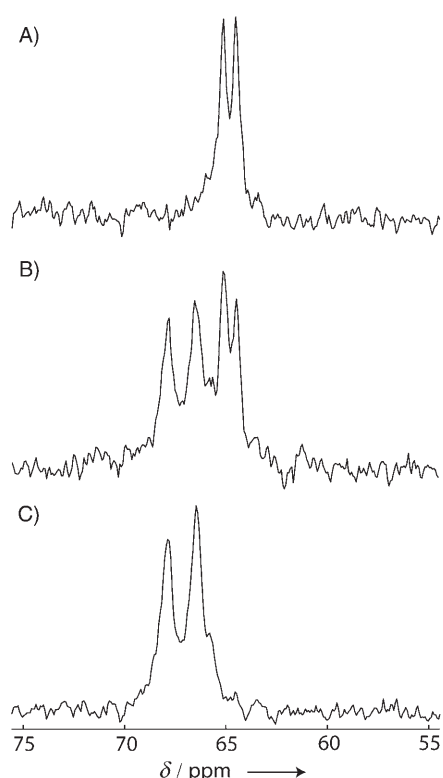
Figure 1. Titration of biosensor **2** with avidin. A) 140 μM **2** with peaks at 65.1 and 64.5 ppm and line widths of 24 and 25 Hz, respectively. B) 126 μM **2** and 16 μM avidin tetramer. C) 109 μM **2** and 29 μM avidin tetramer, corresponding to fully titrated biosensor, with peaks at 67.9 and 66.4 ppm and line widths of 43 and 35 Hz, respectively. All spectra were collected at 23 °C, 16 scans. The two biosensor diastereomers shift downfield and only slightly broaden upon avidin binding of construct **2**.

peak by 2.8 ppm and the upfield peak by 1.9 ppm. Each diastereomer undergoes a different change in chemical shift, thus separation of the diastereomer peaks increases from 0.6 to 1.5 ppm upon avidin binding. Based on calculations by Harris and co-workers, this increase in diastereomer separation might arise from different increases in the electrostatic potential that protein-bound, encapsulated xenon experiences.[8] The difference in biosensor line widths likely arises from biosensor dia-

stereomers having different xenon-binding properties; this was first observed for functionalized cryptophane-A diastereomers by Huber et al.[9]

The xenon spectra for avidin-bound constructs **1** and **2** (Figures S1 and 1, respectively) indicate that a significant source of line width for construct **1** is an increase in the spread of avidin-bound shifts for diastereomer resonances. These data indicate that the protein-bound form of the xenon biosensor can provide a signal-to-noise ratio comparable to that of the protein-free form, and that minimizing the number of biosensor diastereomers is critical for obtaining a good signal-to-noise ratio. For highest sensitivity, the optimal xenon biosensor should consist of a single diastereomer, which can be made by using a pure enantiomer of cryptophane-A.[10]

Linker flexibility

Although the peaks from avidin-bound diastereomers of construct **2** remain fairly sharp (Figure 1), there is a 14 Hz increase in the line width of each peak upon avidin binding. A change in the xenon exchange rate was ruled out as the source of the increased line width for the protein-bound sensor by determining the exchange rates for both protein-free and protein-bound forms.[6] The increase in line width likely arises from correlation-time-dependent relaxation mechanisms. The molecular nature of the linker can be expected to determine the extent of motional coupling between the cage and protein. If the linker acts as a rigid connection between the cage and avidin, then the cage motion will be the same as that of the protein, a correlation time of ~30 ns for the avidin tetramer (see Experimental Section). However, if the linker is flexible then the cage can reorient rapidly, independently of the protein; this leads to a decreased correlation time and narrower line.

The effect of linker rigidity on biosensor line width was determined by characterization of biosensor construct **3**, analogous to **2** but with a six-glycine linker between the cage-peptide and biotin. The six planar peptide bonds in the linker of **3** restrict the rotational motion of the biosensor when it is bound to avidin. Figure 2 shows the spectra of construct **3** in the absence and presence of avidin. In the absence of avidin, there are two narrow peaks, 35 and 24 Hz, separated by 1 ppm, which correspond to the two biosensor diastereomers, *RL* and *LL*. Upon avidin binding, four biosensor peaks of greater line width (45–55 Hz) and unequal intensity appear. The relative amounts of the diastereomers are equal (Figure 2 A), therefore each diastereomer must give rise to one large and one small peak when bound to avidin (Figure 2 B). The source of the two smaller peaks was investigated by preparing a sample in which most of the protein-bound construct **3** was bound at a ratio of one molecule per avidin (see Experimental Section). The corresponding [129]Xe NMR spectrum was similar to that shown in Figure 2 B, but the intensities of the two smaller peaks were significantly diminished (data not shown). This observation and the close proximity of two biotin-binding sites on avidin (Figure 5 A, below) indicate that the smaller peaks in Figure 2 B arise from two biosensor molecules being bound in close proximity. More-flexible linkers, as in **2** and **5**, allow more
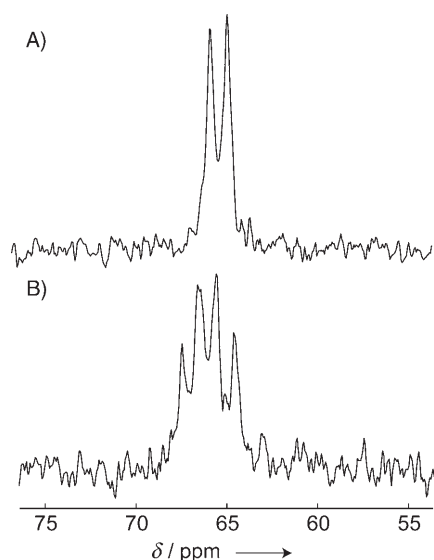
Figure 2. Titration of biosensor **3** with avidin. A) 82 μM **3** with peaks at 65.9 and 65.0 ppm and line widths of 35 and 24 Hz, respectively. B) 77 μM **3** and 20 μM avidin tetramer, corresponding to fully titrated biosensor, with peaks at 67.4, 66.5, 65.6, and 64.5 ppm and approximate line widths of 55, 49, 46, and 57 Hz, respectively. All spectra were collected at 23 °C, 16 scans. Four biosensor resonances appear upon avidin binding of construct **3** from interactions between protein-bound biosensors that are in close proximity.

independent motion of the cage, thus reducing the effects of neighboring ligands on one another. Because this effect might only arise from binding two biosensors in close proximity to each other and can be avoided by using a flexible linker, it was not investigated further.

The increase in line width of ~25 Hz for construct **3** upon avidin binding is larger than that for construct **2** (~14 Hz). This likely arises from an increased correlation time resulting from the more rigid glycine linker. Because linker flexibility affects protein-bound biosensor line width, the conformational constraint from the planar succinimide ring in construct **1** probably makes its behavior less than optimal relative to other linkers of similar length.

Linker length

The correlation time for the avidin-bound biosensor will also be affected by the length of the linker between the cage and the surface of avidin. Even if the linker is flexible, a shorter linker will restrict cage motion due to proximity to the protein surface. Simulations by Sears and Jameson indicate that contact between the protein surface and the cage also influences the chemical shift of the encapsulated xenon.[8] Therefore, a decrease in linker length should also lead to an increase in chemical-shift change upon binding of encapsulated xenon to avidin.

The effect of linker length on biosensor line width and chemical shift was explored by comparing the protein-bound properties of biosensors with three different linker lengths. The three constructs, **2**, **4**, and **5**, have two diastereomers and linkers of comparable flexibility. Construct **2** has an intermediate

linker length, with the cage ~23 Å from the protein surface, and yields two resolved protein-bound resonances that shift by more than 2 ppm and broaden by ~14 Hz upon avidin binding (Figure 1). Construct **4** lacks a linker between biotin and the cage-peptide, so that the cage is ~8 Å from the protein. [129]Xe spectra from free and avidin-bound sensor **4** are shown in Figure 3. The protein-free spectrum shows that there
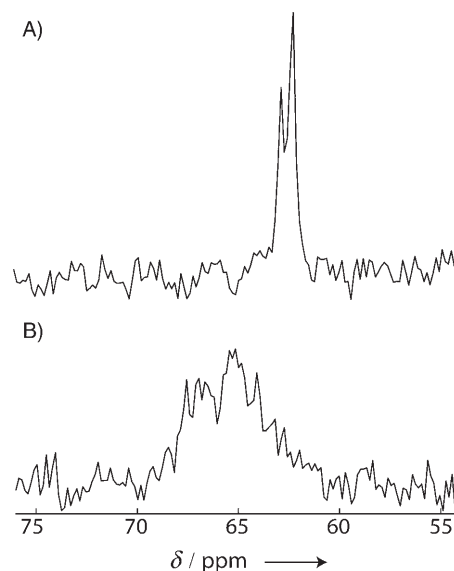
Figure 3. Titration of biosensor **4** with avidin. A) 72 μM of construct **4** with peaks at 62.9 and 62.3 ppm and line widths of 17 and 12 Hz, respectively. B) 72 μM **4** and 18 μM avidin tetramer, corresponding to fully titrated biosensor, with peaks at 67 and 65 ppm and line widths of ~125 Hz. Both spectra were acquired at 20 °C. The protein-free spectrum was acquired with 16 scans, and the protein-bound spectrum was acquired with 64 scans. The unequal intensities of both diastereomers indicate that their relative positions remain the same after protein binding. The broad protein-bound resonances arise from a short linker that restricts the motion of the biosensor.

is an unequal mixture of the two diastereomers, which is most likely a result of the purification process in which a narrow HPLC fraction was collected, partially separating the diastereomers. Comparison with the protein-bound spectrum shows that the upfield and downfield diastereomers retain their relative chemical shifts upon avidin binding. When construct **4** binds avidin, its resonances broaden from ~15 to ~125 Hz and shift from 62.3 and 62.9 ppm to ~65 and ~67 ppm, respectively. The increase in line width of 110 Hz limits the accuracy of the measurement of the change in chemical shift, but it is apparent that the upfield and downfield diastereomers shift by ~3 and ~4 ppm, respectively, which are the largest chemical-shift changes observed for a xenon biosensor. The decrease in linker length correlates with an increase in both line width and chemical-shift sensitivity to avidin binding.

Construct **5** has a linker composed of twelve ethylene glycol units; this puts the cage ~55 Å from the protein surface. When **5** is titrated with avidin, there is no change in the shifts of the xenon biosensor resonances (Figure 4) and the line width narrows slightly from ~28 to ~22 Hz. The lack of line
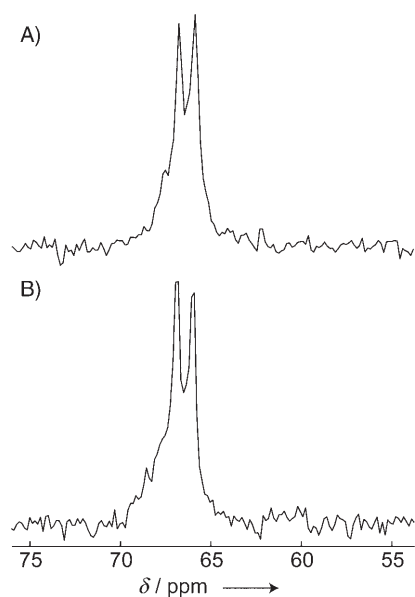
Figure 4. Titration of biosensor **5** with avidin. A) 50 μM **5** with two peaks at 66.9 and 66.1 ppm and line widths of 27 and 31 Hz. B) 50 μM **5** and 13 μM avidin tetramer, corresponding to fully titrated biosensor, with two peaks at 66.9 and 66.0 ppm and line widths of 24 and 20 Hz. There is no change in chemical shift but a slight decrease in line width for construct **5** upon avidin binding due to a long, flexible linker.

width and chemical shift sensitivity of construct **5** to avidin binding indicates that there is a maximal linker length for cage-encapsulated xenon's sensitivity to avidin binding.

To better visualize the protein-bound biosensor, constructs **2**, **4**, and **5** were modeled into the biotin-binding site of avidin.[11] The biosensor was modeled with a fully extended linker, so these models show the maximum distance the cage can be from the surface of the protein. Although these models are not energy-minimized structures, they serve as qualitative comparisons for biosensors with different linker lengths. Figure 5 A and B show a close view of the avidin-bound biosensor model for biosensors **2** and **4**, respectively. For these, the maximum distance the cage can be from the protein surface is ~25 or ~8 Å, respectively. Because the four biotin-binding sites in avidin are asymmetrically distributed, two of the biosensors are in proximity (Figure 5 A). This probably contributes to the restriction of rotational motion of the biosensor. Figure 5 C shows avidin bound to four biosensor **5** molecules, for which the maximum protein-to-cage distance is ~50 Å.

Simulations by Sears and Jameson reproduced the magnitude and direction of the chemical-shift change of the xenon biosensor upon avidin binding by decreasing the internal volume of the cage.[8] Their results indicate that contact of the cage with the protein surface might be the primary mechanism of xenon biosensor chemical-shift sensitivity to avidin binding. Although none of the biosensors studied

has a short enough linker to cause the cage to be in direct contact with the surface of the protein all of the time, the inverse proportionality between the linker length and chemical-shift sensitivity is in agreement with a contact-mediated binding-induced shift.

Partial cage deuteration

The increase in line width for biosensor resonances when bound to protein indicates that there is an increase in T_2 relaxation rate upon protein binding. An increase in the rate of xenon exchange into the cage has been previously ruled out as a source of relaxation.[6] The likely relaxation mechanisms are dipole–dipole coupling and chemical-shift anisotropy (CSA).

The contribution of dipole–dipole coupling between encapsulated xenon and cage protons can be calculated by using the estimated correlation time of the xenon biosensor (see Experimental Section) and the xenon–proton internuclear distances that have been previously reported for cryptophane-A dissolved in $(CDCl_2)_2$ based on SPINOE measurements.[12] The validity of the assumption that the internuclear distances do not significantly change when the cage is functionalized, dissolved in water, and bound to avidin will be discussed below. The rate of proton–xenon cross relaxation for the biosensor can be
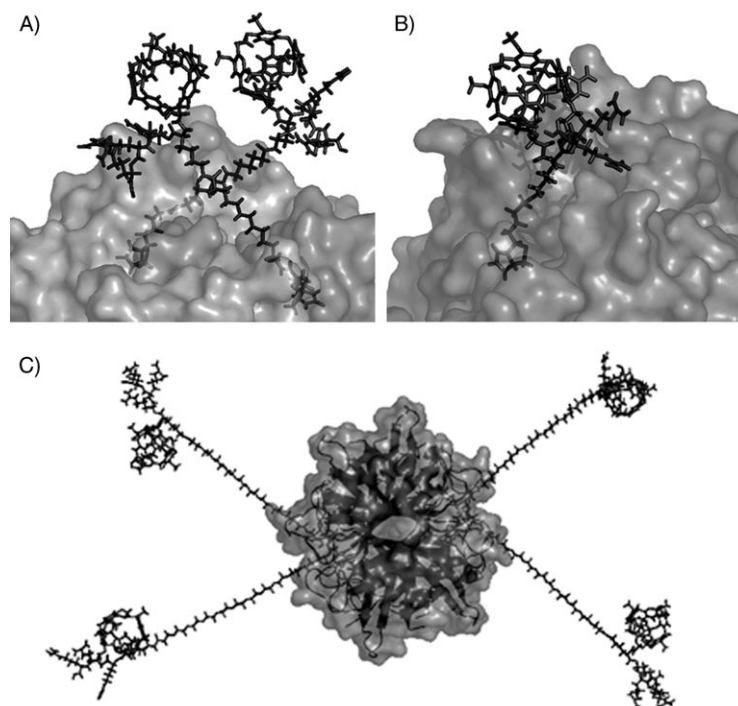
Figure 5. Molecular models of the xenon biosensor bound to avidin. A) Two biosensor **2** molecules bound to avidin (space-filling). The proximity of two biotin-binding sites allows for the interaction of two biosensor molecules when bound to avidin. The linker of construct **2** keeps the cage within ~23 Å of the protein surface. B) One biosensor **4** molecule bound to avidin (space-filling). The second biosensor molecule is not shown for clarity. The linker of construct **4** keeps the cage within ~8 Å of the protein surface and in proximity to the second cage and protein surface. C) Four biosensor **5** molecules bound to avidin (space-filling with cartoon backbone). The linker of construct **5** extends the cage ~50 Å from the protein surface.

calculated using the following relationships:

$$\sigma_{HXe} = \sum_i \sigma_{HXe}(i) \tag{1a}$$

$$\sigma_{HXe}(i) = \frac{d_{00}}{8}\{4J(0) + J(\omega_H - \omega_{Xe}) + 3J(\omega_{Xe}) + 6J(\omega_H) + 6J(\omega_H + \omega_{Xe})\} \tag{1b}$$

with

$$d_{00} = \left(\frac{\mu_0 \hbar \gamma_H \gamma_{Xe}}{4\pi}\right)^2 \left\langle \frac{1}{r(i)^6} \right\rangle \tag{1c}$$

and

$$J(\omega) = \frac{2\tau_c}{5(1 + \omega^2 \tau_c^2)} \tag{1d}$$

where σ_{HXe} is the total proton–xenon cross relaxation rate, $\sigma_{HXe}(i)$ is the proton–xenon cross relaxation rate for the ith proton, $r(i)^6$ is the internuclear distance for the ith proton, and τ_c is the correlation time for rotation of the biosensor.[13] The $\langle r(i)^{-6} \rangle$ values that have been previously determined[12] were used to calculate estimates of σ_{HXe} for the protein-free biosensor, with $\tau_c \sim 1.6$ ns, and the protein-bound biosensor, with $\tau_c \sim 30$ ns (Experimental Section). σ_{HXe} is 0.07 Hz and 0.8 Hz for the protein-free and protein-bound biosensors, respectively. These predicted values for dipolar broadening are well below the experimental values; this indicates that H–Xe dipole–dipole coupling does not contribute significantly to biosensor relaxation.

The contribution of dipole–dipole coupling to biosensor line width was also tested experimentally by using a partially deuterated version of construct **2**, designated **2***, in which the methoxy and linker protons were deuterated (Scheme 1). The calculated differences in σ_{HXe} values predicted for partially deuterated free and avidin-bound **2*** (0.03 and 0.4 Hz) are within the error of line-width measurement (4 Hz); this indicates that the line widths of **2*** and **2** should be the same. Comparison of the line widths of free and avidin-bound **2*** (~19 and ~37 Hz, respectively, Figure S2) with those for construct **2** (~24 and ~39 Hz) indicates that dipole–dipole coupling does not contribute significantly to protein-bound line width. This is a result of the relatively large average proton–xenon internuclear distance for encapsulated xenon (5 ± 0.7 Å) leading to weak dipolar coupling because of the $\langle r(i)^{-6} \rangle$ dependence.

Temperature dependence

The contribution of xenon exchange to biosensor line width was probed by measuring the temperature dependence of free and avidin-bound biosensor resonances for construct **2***. As shown in Figure 6, both the line width and chemical shift of the xenon biosensor depend on temperature. The chemical shift of construct **2*** for both free and avidin-bound forms depends linearly on temperature between 10 and 40 °C with a slope of 0.27 ppm °C^{-1} (Figure S3); this is the same as that for cryptophane-A-encapsulated xenon in deuterated tetrachloro-
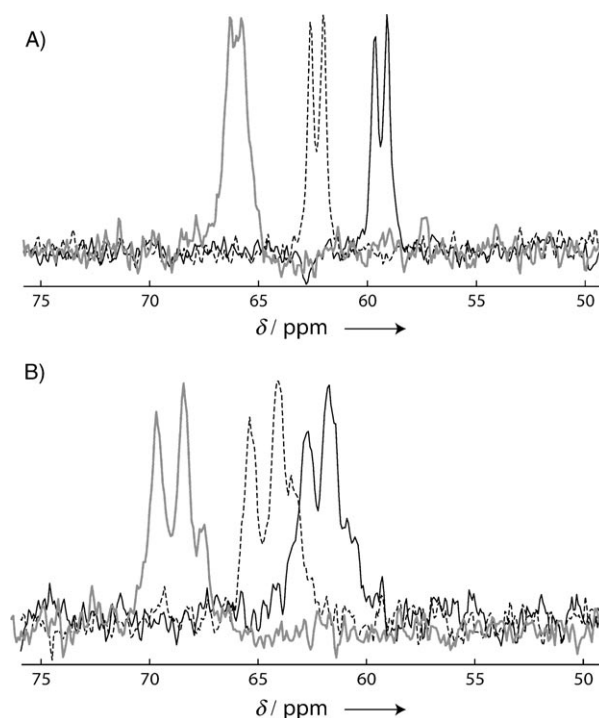
Figure 6. Temperature dependence for the ^{129}Xe NMR spectra of A) 105 μM avidin-free and B) 87 μM avidin-bound construct **2***. Spectra for three different temperatures are shown, 35 °C (gray line), 20 °C (dashed line), and 10 °C (black line). The line widths of free ^{129}Xe in solution were between 10 and 20 Hz at all temperatures. The spectra were collected with four scans for (A) and eight scans for (B). At temperatures above 25 °C, the protein-free biosensor resonance broadens due to xenon exchange. The line width of the protein-bound biosensor is essentially temperature independent over the 10–35 °C range.

ethane (~0.28 ppm °C^{-1}).[14] The temperature dependence of encapsulated xenon is thought to arise from increased xenon sampling of the repulsive regions of the xenon–cryptophane potential and an increase in cryptophane-A molecules in higher-energy conformations.[14,15] The similarity of temperature-dependent chemical shift for cryptophane-A dissolved in $(CDCl_2)_2$ and cryptophane-A that has been functionalized, dissolved in water, and protein-bound suggests that the structure and interactions of the cage and encapsulated xenon are similar in these different environments. This supports the previous assumption that the internuclear distances between encapsulated xenon and cage protons are similar in different constructs and solvents.

As shown in Figure 6, the line width for avidin-free construct **2*** increases significantly with temperature above 25 °C; this indicates that the exchange rate reaches ≥ 30 s^{-1}, so exchange broadening significantly contributes to protein-free biosensor line width (see also Figure S4a). From 10 to 25 °C, the biosensor line width decreases slightly with temperature; this indicates that correlation-time-dependent mechanisms dominate at these temperatures. Figure 6 also shows that the line width of the protein-bound biosensor **2*** is not significantly temperature dependent from 10 to 35 °C; this indicates that a relaxa-

tion mechanism other than exchange must dominate at low temperatures (see also Figure S4 b).

Similar measurements were made for the avidin-free and avidin-bound forms of constructs **3** and **5**. The line width and chemical shift for the avidin-free form of construct **3** and both the avidin-free and avidin-bound forms of construct **5** exhibited similar behavior to that observed for the avidin-free form of construct **2***. However, the resonances for the avidin-bound form of construct **3** were narrowest at 23 °C and broadened when the temperature was increased or decreased by 10 °C (Figure S5), again this indicates a combination of mechanisms as for **2***.

The temperature dependence of the line width for construct **2*** was used to determine the xenon exchange rates above 25 °C for protein-free biosensor. Exchange affects line width according to the relationship

$$\Delta \nu_{1/2} = (\pi \tau_{ex})^{-1} \qquad (2)$$

where $\Delta \nu_{1/2}$ is the contribution to the line width at half height and τ_{ex} is the exchange rate. To calculate τ_{ex}, the line widths at high temperature were corrected for line-width contribution from the low-temperature relaxation mechanisms by extrapolating the temperature-dependent behavior between 10 and 25 °C up to 35 °C. The exchange contributions to line widths were used to calculate τ_{ex} at 28, 30, and 35 °C. For temperatures below 25 °C, τ_{ex} was determined by measuring the recovery of selectively saturated xenon signals, as described previously.[6] The temperature-dependent exchange rates were used to obtain an activation energy for xenon dissociation from the cryptophane complex in water of 121 ± 7 kJ mol^{-1}. This is approximately three times higher than that determined for xenon–cryptophane-A decomplexation in $(CDCl_2)_2$ of 37 kJ mol^{-1},[16] one cause of which might be a higher enthalpic cost for the dissolution of xenon in water.

Other relaxation contributions for the protein-bound biosensor

The dipolar (~1 Hz) and exchange (~7 Hz) contributions to the line widths for xenon in the protein-bound biosensor **2** are not sufficient to explain the observed value of ~32 Hz (corrected for inhomogeneous broadening from field inhomogeneity estimated from the ^{1}H line width in D$_2$O in the sample). Chemical-shift anisotropy (CSA) was also considered as a possible contributing mechanism. The contribution of CSA to xenon line width can be significant due to the extraordinary chemical shift sensitivity of xenon to its local environment. The CSA value required for a given line width can be calculated from the following relationship:

$$R_2 = \frac{1}{18} \{ \Delta \sigma_{CSA}^2 \omega_{Xe}^2 (4J(0) + 3J(\omega_{Xe})) \} \qquad (3)$$

where (R_2) is the line width in Hz, $\Delta \sigma_{CSA}$ is the chemical-shift anisotropy in ppm, ω_{Xe} is the resonant frequency of ^{129}Xe at 7 T (2π* 82.9 MHz), and $J(\omega)$ is estimated from the correlation time, Equation (1d).[13] By using the ~30 ns estimated τ_c for the avidin-bound biosensor **2*** and the 24 Hz observed excess line width, a $\Delta \sigma_{CSA}$ value of ~180 ppm was calculated. This value seems unrealistically large for xenon inside a deformed cryptophane-A cage. Reported ^{129}Xe CSA values range from 10 ppm to over 150 ppm, but those larger than tens of ppm are for xenon inside fully occupied nanochannels where xenon–xenon interactions dominate the CSA term.[17] Further experiments are needed to directly establish the protein-bound crypto-phane-encapsulated ^{129}Xe CSA.

Another possible contribution to bound biosensor line width is conformational exchange. The fact that multiple peaks are seen for bound biosensor **3** (Figure 2) and a small upfield peak is seen for protein bound biosensor **2** (Figures 1C, S2C) emphasizes the sensitivity of encapsulated ^{129}Xe to local interactions. It is possible that slow (ms–μs) fluctuations among multiply bound conformations also contribute to the line width for other biosensors. Studies of other linkers, and proteins with single binding sites, are probably needed to resolve this issue.

Conclusion

Optimizing the design of the xenon biosensor construct has allowed signals from avidin-bound biosensor diastereomers to be resolved, thus demonstrating the feasibility of obtaining narrow lines from protein-bound xenon biosensors. The structural details of the biosensor linker significantly influence the line width and chemical-shift sensitivity of the protein-bound xenon biosensor. The characteristics of the constructs surveyed here indicate that a flexible linker of moderate length, such as that used in constructs **2** or **5**, can lead to reasonably narrow lines for protein-bound xenon biosensors. Depending on the desired application, the chemical-shift sensitivity of the xenon biosensor can be tuned by using a shorter or longer linker. The relaxation mechanisms that contribute to the line width for the avidin-bound biosensor include bulk-to-cage xenon exchange, biosensor conformational exchange, and possibly CSA. The exchange contribution is inherent, since xenon must be able to enter the cage for the biosensor to function; however, it might be possible to modify the cage to decrease the rate of exchange without significantly altering the xenon-binding affinity. Conformational-exchange contributions seem to be eliminated in biosensor molecules with longer, flexible linkers. They might also disappear for targets with single biosensor-binding sites. Understanding the parameters for obtaining good signal-to-noise ratios for protein-bound, cryptophane-encapsulated xenon is critical for applications that require protein functionalization, such as affinity targeting with antibodies[7, 18] or metabolite sensing with engineered periplasmic binding proteins,[19] at in vivo concentrations.

Experimental Section

Cryptophane-A carboxylic acid[6] and partially deuterated cryptophane-A carboxylic acid[20] were synthesized as previously described. The complete syntheses of constructs **1**[6] and **3**[21] have

been previously described. For constructs **2** and **4**, the cryptophane-A carboxylic acid was attached to the deprotected N terminus of a hydrophilic peptide [NH$_2$K(Cbz)R(Pbf)K(Boc)R(Pbf)CO$_2$Me)] by using benzotriazole-1-yl-oxytrispyrrolidinophosphonium hexafluorophosphate (PyBOP) and *N*-methylmorpholine in dimethylformamide (DMF). The peptide was synthesized by conventional solid-phase peptide chemistry with trityl resin (Fmoc chemistry; PyBOP/diisopropylethylamine (DIEA) acylation; deprotection with 20% piperidine in DMF; resin cleavage with AcOH/trifluoroethanol/CH$_2$Cl$_2$ (1:1:8); esterification of the C terminus by using diazomethane; deprotection of the N terminus with piperidine in DMF; purification by reversed-phase HPLC). The Cbz protecting group was then cleaved under hydrogenation conditions (H$_2$, Pd/C). The cryptophane-A–peptide construct was biotinylated by treating the unprotected lysine side chain with NHS-LC-LC-biotin (Pierce Chemical, Rockford, IL, USA) in DMF in the presence of DIEA (for construct **2**) or with biotin (for construct **4**), deprotected with trifluoroacetic acid (TFA)/Me$_2$S/thioanisole (18:1:1), and purified by reversed-phase HPLC. For construct **5**, the cryptophane-A carboxylic acid was attached to the deprotected terminus of a small hydrophilic peptide [KR$_3$COOH] that had been synthesized by conventional solid-phase methods (Fmoc chemistry; dicyclohexyl carbodiimide/*N*-hydroxybenzotriazole (HOBt)/1-methyl-2-pyrrolidone (NMP) acylation; deprotection in TFA with water/thioanisole. The purity of the crude product was >95% by FTICR-MS). The cage-peptide construct was biotinylated by treatment with 2-(1*H*-benzotriazole-1-yl)-1,1,3,3-tetramethyluronium hexafluorophosphate (HBTU)/HOBt/DIEA/N-Fmoc-amino-dPEG$_{12}$-acid (Quanta Biodesign, Powell, OH, USA), deprotected with piperidine/NMP, and treated with HBTU/HOBT/DIEA/biotin.

All ^{129}Xe NMR spectroscopy was conducted by using the stopped-flow bubble-mode apparatus, a 300 MHz (proton frequency) Varian Inova spectrometer, and an Amersham Health ^{129}Xe polarizer, which produced ~3% polarized ^{129}Xe, as previously described.[21] All spectra were referenced to xenon gas at 0 ppm, fitted by matNMR, and processed with a 10 Hz exponential filter, unless otherwise noted. The solution peak for all spectra was at 191 ppm for solutions in D$_2$O/H$_2$O (50:50) and at 189 ppm for solutions in 99% D$_2$O, and typically had a line width of ~10 Hz. The longitudinal relaxation time for ^{129}Xe in biosensor samples was ~1 min. Unless otherwise noted, errors for chemical shifts were ±0.1 ppm, and line widths were ±4 Hz. The chemical shift of the solution-dissolved xenon peak changed with temperature by less than 0.04 ppm °C^{-1} between 10 and 40°C. Propan-1-ol (~10%) was added to biosensor solutions for constructs **3** and **5** to suppress sample foaming during xenon bubbling. Sample concentrations were determined by UV/Vis spectrophotometry with molar-absorptivity coefficients of 8000 M^{-1} for pure biosensor[6] and 96000 M^{-1} for pure avidin (Sigma).[22] The sample in which one molecule of construct **3** was bound per avidin was prepared by adding construct **3** (1 equiv) to a dilute aqueous solution of avidin tetramer (2 equiv), or biotin-binding sites (8 equiv), during mixing. Because the biotin-binding sites were in excess and avidin binds biotin in a noncooperative manner,[23] most biosensor was assumed to be bound at a ratio of one molecule per avidin.

Molecular models of the biosensor constructs were built with PyMOL[24] and docked into the crystal structure of biotin-bound avidin[11] by overlaying the biosensor-tethered biotin with avidin-bound biotin and positioning the biosensor linker in the biotin-binding channel. No energy minimization on the biosensor or biosensor–avidin construct was performed.

The correlation times of the protein-free and protein-bound biosensor can be estimated according to the following relationships.

$$\tau_C = \frac{4\pi\eta_W r_H^3}{3k_B T} \tag{4a}$$

$$r_H = \left(\frac{3\bar{V}M_r}{4\pi N_A}\right)^{1/3} + r_W \tag{4b}$$

Here τ_c is the correlation time, η_W is the viscosity of water, r_H is the effective radius, $\bar{V}$ is the specific volume, M_r is the molecular weight, and r_W is the thickness of a single hydration sphere for water.[13] Accordingly, the correlation times for the avidin-free ($M_r = $ ~2 kDa) and avidin-bound ($M_r = $ ~74 kDa) xenon biosensor were calculated to be ~1.6 and ~30 ns, respectively.

[1] J. M. Perez, L. Josephson, T. O'Loughlin, D. Hogemann, R. Weissleder, *Nat. Biotechnol.* **2002**, *20*, 816–820.

[2] A. Y. Louie, M. M. Huber, E. T. Ahrens, U. Rothbacher, R. Moats, R. E. Jacobs, S. E. Fraser, T. J. Meade, *Nat. Biotechnol.* **2000**, *18*, 321–325.

[3] K. Golman, J. H. Ardenaer-Larsen, J. S. Petersson, S. Mansson, I. Leunbach, *Proc. Natl. Acad. Sci. USA* **2003**, *100*, 10435–10439.

[4] a) M. S. Albert, G. D. Cates, B. Dreihuys, W. Happer, B. Saam, C. S. Springer, A. Wishnia, *Nature* **1994**, *370*, 199–201; b) M. S. Chawla, X. J. Chen, H. E. Moller, G. P. Cofer, C. T. Wheeler, L. W. Hedlund, G. A. Johnson, *Proc. Natl. Acad. Sci. USA* **1998**, *95*, 10832–10835.

[5] M. M. Spence, S. M. Rubin, I. E. Dimitrov, E. J. Ruiz, D. E. Wemmer, A. Pines, S. Q. Yao, F. Tian, P. G. Schultz, *Proc. Natl. Acad. Sci. USA* **2001**, *98*, 10654–10657.

[6] M. M. Spence, E. J. Ruiz, S. M. Rubin, T. J. Lowery, N. Winssinger, P. G. Schultz, D. E. Wemmer, A. Pines, *J. Am. Chem. Soc.* **2004**, *126*, 15287–15294.

[7] T. J. Lowery, S. M. Rubin, E. J. Ruiz, M. M. Spence, N. Winssinger, P. G. Schultz, A. Pines, D. E. Wemmer, *Magn. Reson. Imaging* **2003**, *21*, 1235–1239.

[8] D. N. Sears, C. J. Jameson, R. A. Harris, *J. Chem. Phys.* **2004**, *120*, 3277–3283.

[9] J. G. Huber, L. Dubois, H. Desvaux, J. P. Dutasta, T. Brotin, P. Berthault, *J. Phys. Chem. A* **2004**, *108*, 9608–9615.

[10] T. Brotin, R. Barbe, M. Darzac, J. P. Dutasta, *Chem. Eur. J.* **2003**, *9*, 5784–5792.

[11] L. Pugliese, A. Coda, M. Malcovati, M. Bolognesi, *J. Mol. Biol.* **1993**, *231*, 698–710.

[12] M. Luhmer, B. M. Goodson, Y. Q. Song, D. D. Laws, L. Kaiser, M. C. Cyrier, A. Pines, *J. Am. Chem. Soc.* **1999**, *121*, 3502–3512.

[13] J. Cavanagh, W. J. Fairbrother, A. G. Palmer III, N. J. Skelton, *Protein NMR Spectroscopy*, Academic Press, San Diego, **1996**, pp. 17–18, 267–279.

[14] K. Bartik, M. Luhmer, J. P. Dutasta, A. Collet, J. Reisse, *J. Am. Chem. Soc.* **1998**, *120*, 784 – 791.

[15] D. N. Sears, C. J. Jameson, *J. Chem. Phys.* **2003**, *119*, 12 231 – 12 244.

[16] T. Brotin, J. P. Dutasta, *Eur. J. Org. Chem.* **2003**, 973 – 984.

[17] C. J. Jameson, *J. Chem. Phys.* **2002**, *116*, 8912 – 8929, and references therein.

[18] D. A. Sipkins, D. A. Cheresh, M. R. Kazemi, L. M. Nevin, M. D. Bednarski, K. C. P. Li, *Nature Med.* **1998**, *4*, 623 – 626.

[19] L. L. Looger, M. A. Dwyer, J. J. Smith, H. W. Hellinga, *Nature* **2003**, *423*, 185 – 190.

[20] T. Brotin, A. Lesage, L. Emsley, A. Collet, *J. Am. Chem. Soc.* **2000**, *122*, 1171 – 1174.

[21] S.-I. Han, S. Garcia, T. J. Lowery, E. J. Ruiz, J. A. Seeley, L. Chavez, D. S. King, D. E. Wemmer, A. Pines, *Anal. Chem.* **2005**, *77*, 4008 – 4012.

[22] N. M. Green, *Methods Enzymol.* **1990**, *184*, 51 – 57.

[23] C. Rosano, P. Arosio, M. Bolognesi, *Biomol. Eng.* **1999**, *16*, 5 – 12.

[24] D. L. DeLano, *The PyMol Molecular Graphics System*, DeLano Scientific, San Carlos, CA, **2002**.